

## **S1 Homogeneity analysis of streamflow series**

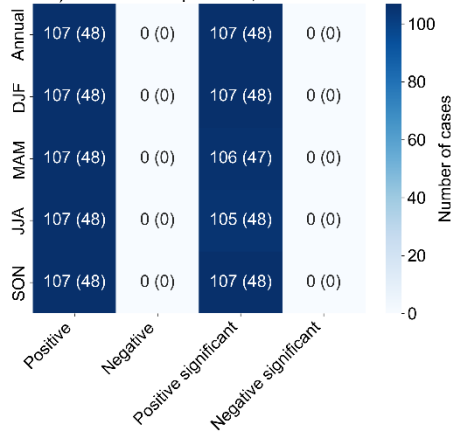
To assess the homogeneity of streamflow records from the LamaH-Ice dataset, we performed the standard Pettitt's test (Pettitt, 1979). Our approach to considering or omitting inhomogeneous series aligns with that of the Norwegian Water Resources and Energy Directorate's method for selecting reference streamflow series for climate change studies (Fleig et al., 2013). The homogeneity analysis revealed that one timeseries needed to be omitted (Syðri-Bægisá river).

Pettitt's test (Pettitt, 1979) is a non-parametric change-point detection test derived from the Mann-Whitney two-sample test. We computed Pettitt's test for each streamflow gauge using the PyHomogeneity Python package (Hussain et al., 2023), setting the significance level at 0.05 and the number of Monte Carlo simulations used to approximate the significance of the test at 20,000. We applied the test to series for annual average streamflow, temperature and precipitation series. In cases where the test indicated a change-point in annual average streamflow, we manually inspected the streamflow series for breaks in homogeneity that were either 1) linked to a documented change in measurement practices or to incidents that compromised data quality, or 2) distinctly observable in the data, and these breaks could not be accounted for by breaks in temperature or precipitation.

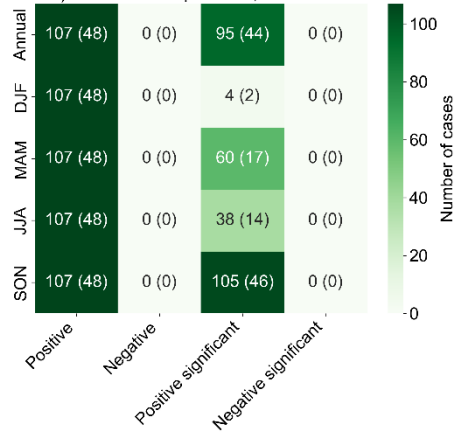
## **S2 Summary and validity of trends in ERA5-Land**

### **S2.1 Summary of trends**

a) Trends in temperature, 1973-2023



b) Trends in temperature, 1993-2023



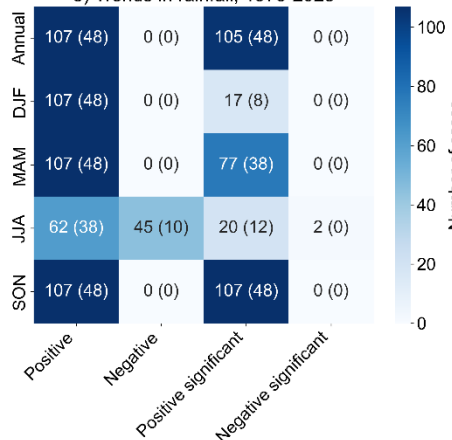
c) Trends in precipitation, 1973-2023



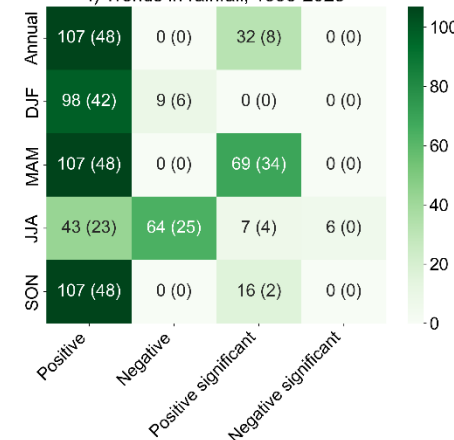
d) Trends in precipitation, 1993-2023



e) Trends in rainfall, 1973-2023



f) Trends in rainfall, 1993-2023



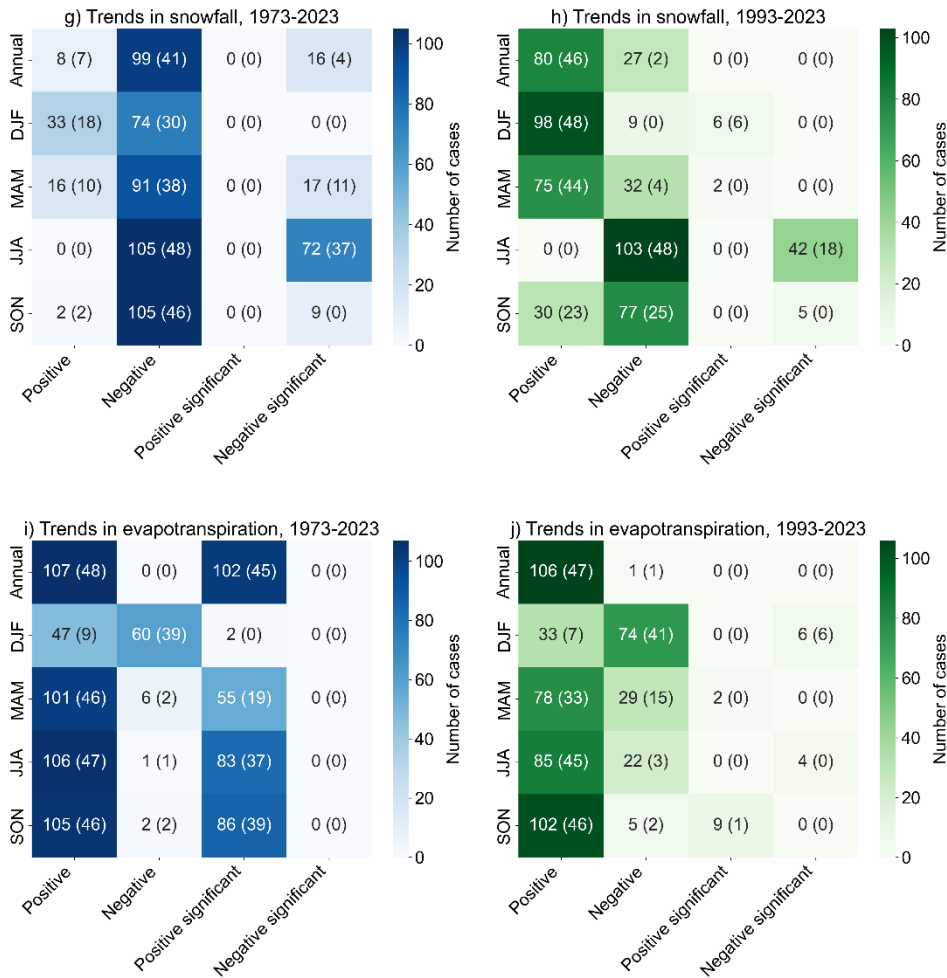


**Figure S1: Heatmaps showing a summary of the results from analysis of annual and seasonal trends in streamflow for the periods 1973-2023 (a) and 1993-2023 (b). The numbers in parentheses indicate the count of catchments with more than 5% glaciation.**

## 30 S2.2 Validity of trends

### Temperature:

To assess the suitability of ERA5-Land for long-term temperature trend analysis in Iceland, we compared reanalysis-derived temperature series with in-situ observations from the Reykjavík weather station. The selected catchment, Korpa River (ID 58), is located in Reykjavík, with the streamflow gauge situated approximately 7 km from the weather station.

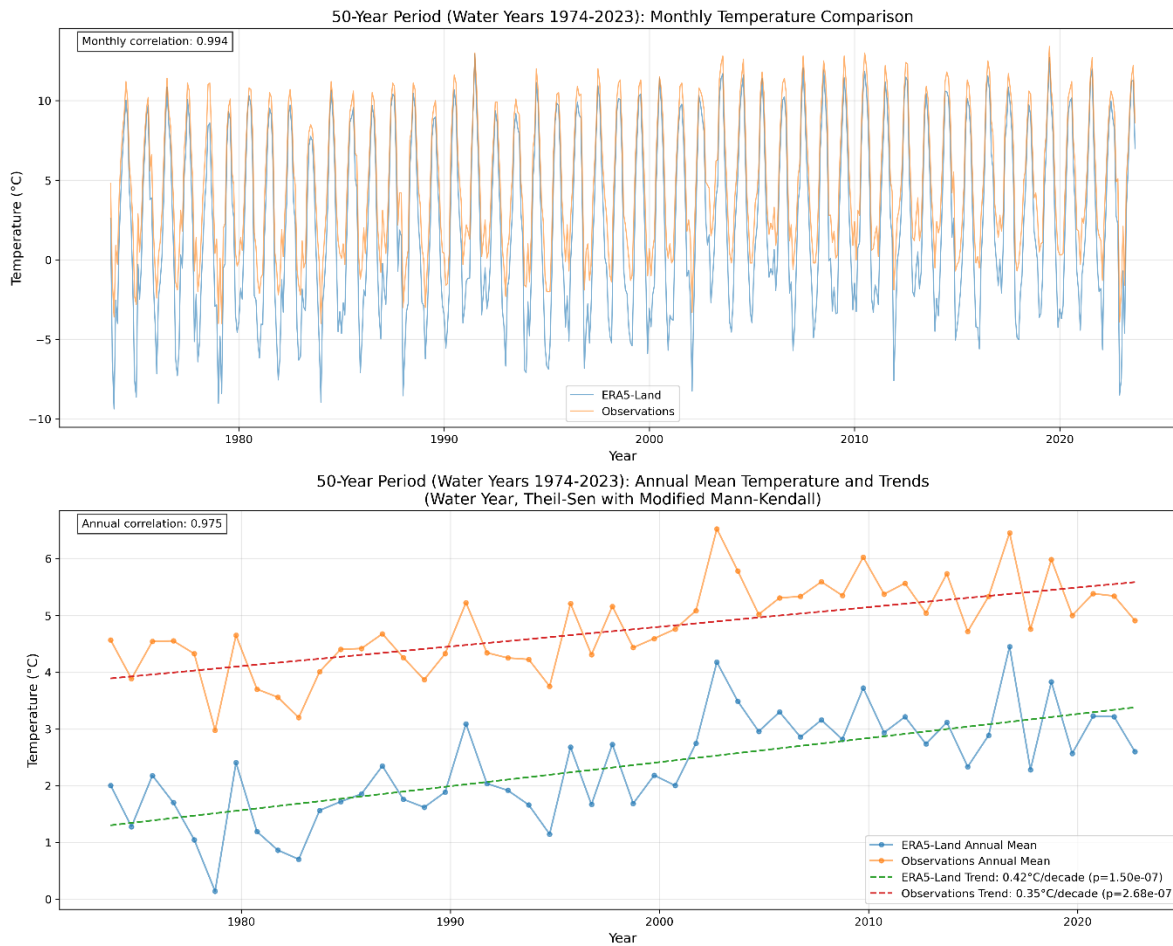


**Figure S2: Comparison of observed temperature series in Reykjavík and catchment-averaged ERA5-Land series for the Korpa catchment (ID 58), located near Reykjavík, over the 1974–2023 period. The top panel shows monthly mean temperatures, and the bottom panel displays annual mean temperatures with Theil-Sen trend lines and associated p-values based on the modified Mann-Kendall test.**

The comparison reveals a good agreement between ERA5-Land and observed monthly temperature series, with a Pearson correlation coefficient of 0.994. Annual mean temperatures also show strong agreement ( $r = 0.975$ ). Both datasets exhibit statistically significant warming over the 50-year study period. The Theil-Sen slope estimates indicate a warming trend of 0.42°C per decade for ERA5-Land and 0.35°C per decade for observations, both with p-values  $< 0.001$ . The temperature series from ERA5-Land is cooler than the observed series, reflecting the higher average elevation of the catchment (171 m a.s.l.) compared to the weather station elevation (60 m a.s.l.). These findings confirm that ERA5-Land effectively captures interannual variability and long-term temperature trends at this site, supporting its use in hydrological and climate analyses across Iceland.

To assess potential temperature biases in ERA5-Land, we compared its mean annual temperature over the period 1973–2018 with that of the regional atmospheric reanalysis CARRA. CARRA has been compared extensively with measurements in

Iceland, showing a good comparison for temperature and precipitation (Rögnvaldsson et al., 2025). We performed the comparison for 107 catchments in the LamaH-Ice dataset, and results are presented in Figure S3.

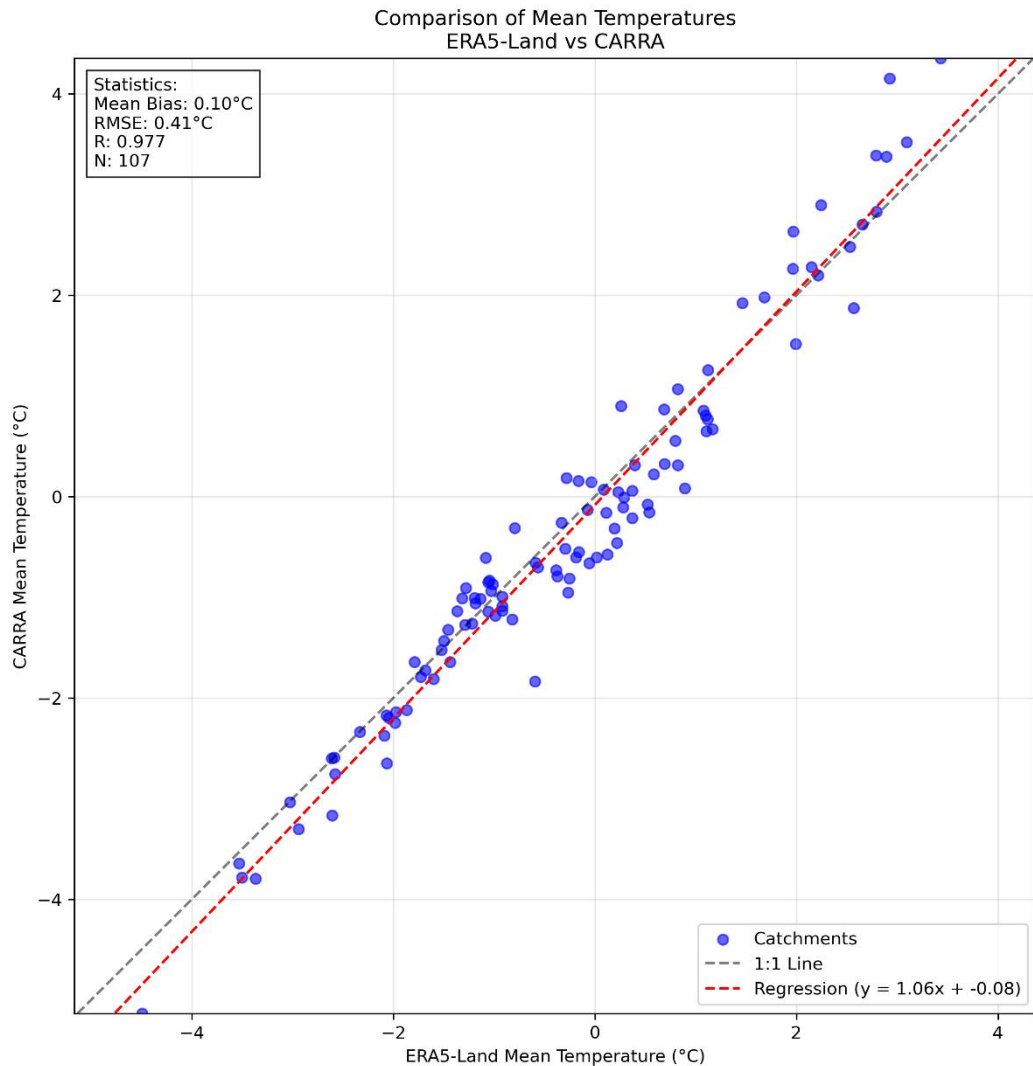


**Figure S3: Comparison of mean annual temperatures between the ERA5-Land and CARRA reanalysis datasets for 107 catchments in LamaH-Ice during the period Oct 1 1973 – Sept 30 2023. The gray dashed line represents the 1:1 relationship, while the red dashed line shows the linear regression ( $y = 1.06x - 0.08$ ). Each point represents one catchment, with temperatures ranging from approximately -4°C to +3°C.**

ERA5-Land exhibits a slight warm bias compared to CARRA, with a mean difference of +0.1°C, a root mean squared error (RMSE) of 0.41°C, and a pearson correlation coefficient of 0.98. The bias is temperature-dependent: ERA5-Land tends to be slightly colder than CARRA at low temperatures (below -1.5°C), and slightly warmer at higher temperatures. Despite this minor systematic difference, the strong agreement between the two datasets supports the suitability of ERA5-Land for analyzing long-term temperature trends in Iceland.

**Precipitation:**

Direct comparisons between reanalysis-based precipitation estimates and gauge observations in cold regions are challenging  
65 due to significant measurement uncertainties, particularly undercatch during snowfall and windy conditions. Because  
systematic corrections are not uniformly applied to Icelandic precipitation records, station-based trends may not provide a  
reliable reference for evaluating reanalysis products. In the comparison by Rögnvaldsson et al. (2025) between CARRA-  
simulated precipitation and gauge measurements, data were carefully filtered to include only observations made under wind  
speeds below 8 m s<sup>-1</sup> and air temperatures above 2 °C. Under these conditions, CARRA performed well, exhibiting only a  
70 slight positive bias of approximately 9% over 1999–2024. Moreover, CARRA has been shown to accurately reproduce winter  
precipitation on Icelandic glaciers (cite).

To assess the validity of ERA5-Land precipitation trends, we compared them with trends derived from the Copernicus Arctic  
Regional Reanalysis (CARRA), a high-resolution (2.5x2.5 km) regional reanalysis. Figure S3 presents precipitation trends (%  
per decade) from both ERA5-Land (left) and CARRA (center) over the 1993–2023 period, alongside a scatter plot comparing  
75 trends between the two datasets (right).

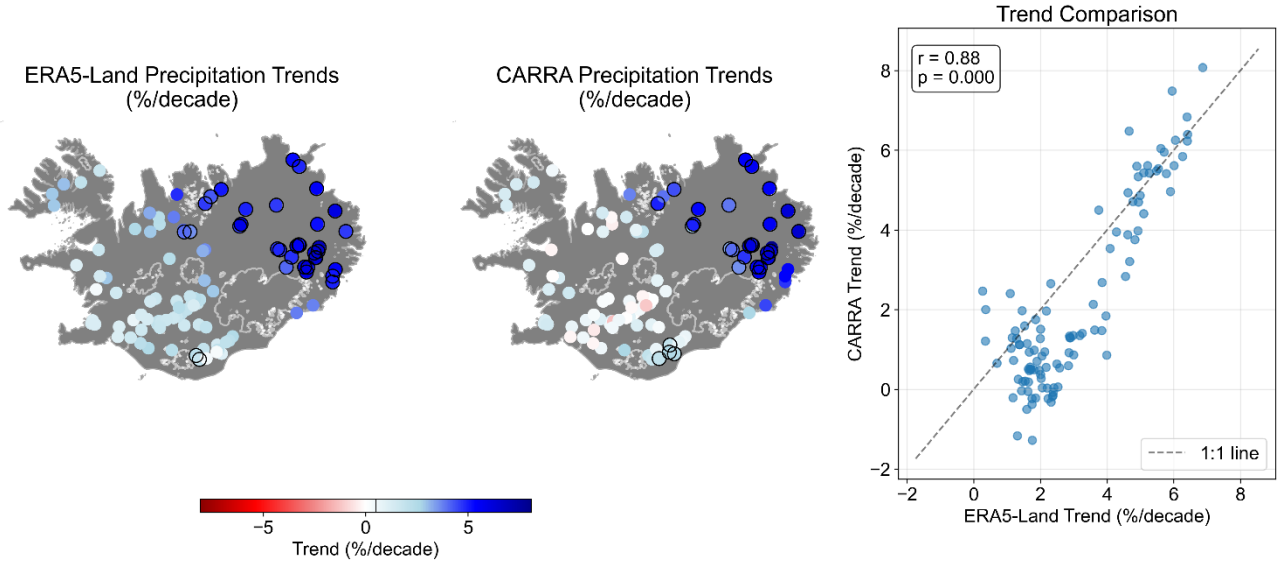


**Figure S4: Comparison of precipitation trends (% per decade) over Iceland for the 1993–2023 period from ERA5-Land (left) and CARRA (center). Each point represents a catchment in the LamaH-Ice dataset. Black circles around gauges indicate statistically significant trends. The right panel shows a scatter plot comparing ERA5-Land and CARRA trends, with the dashed 1:1 line indicating perfect agreement.**  
80

Both datasets show consistent spatial patterns in precipitation trends across Iceland. In particular, both reanalyses indicate increasing precipitation trends in the east and northeast, transitioning to decreasing or near-zero trends toward the southwest. This spatial coherence strengthens confidence in the qualitative pattern of change. However, ERA5-Land generally exhibits  
85 slightly larger trend magnitudes than CARRA. This is reflected in the scatter plot, where most points fall below the 1:1 line.

The correlation between the two datasets is strong ( $r = 0.88$ ,  $p < 0.000$ ), suggesting a high level of agreement in relative trend patterns, even if the magnitudes differ. These results suggest that ERA5-Land captures the broad spatiotemporal distribution of precipitation trends in Iceland and is suitable for use in large-scale hydrological trend assessments, such as those in LamaH-Ice.

90 **S3 Changes in evapotranspiration compared to changes in precipitation**

Figure S5 shows a comparison between trends in precipitation and ET in Iceland.

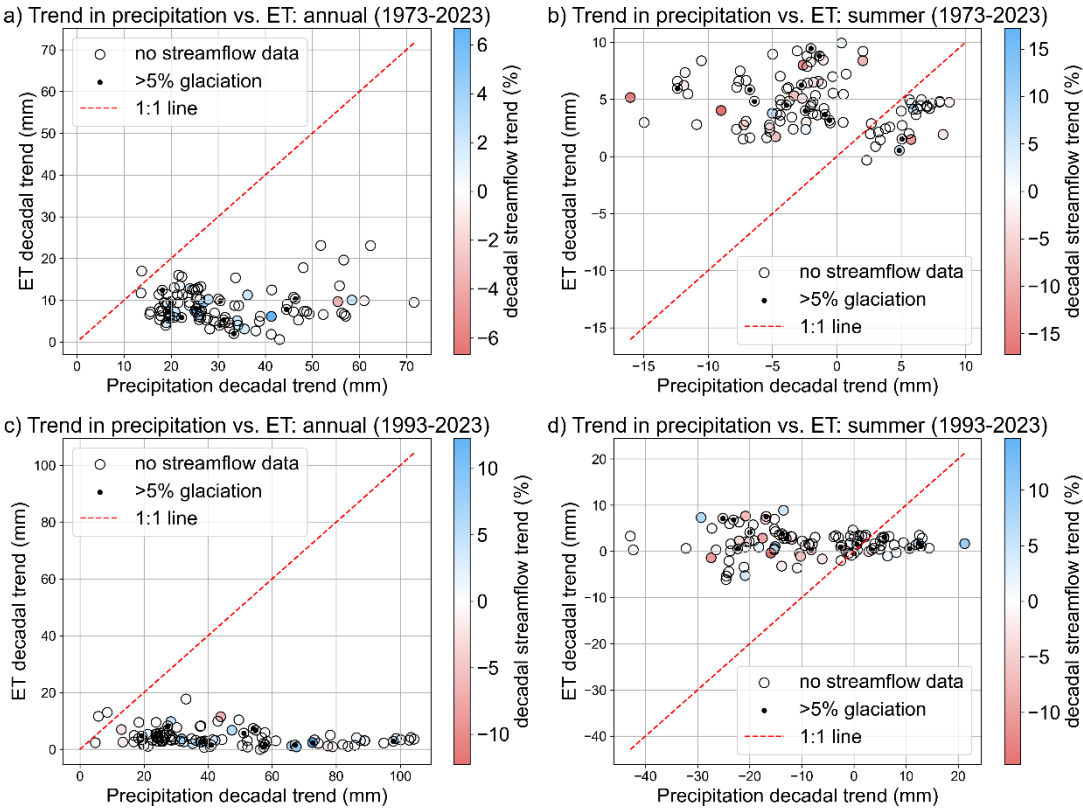


**Figure S5: The trend in precipitation (x-axis) plotted against the trend for evapotranspiration (ET: y-axis) for period 1 (a and b) and period 2 (c and d). Annual trends are shown in panels a and c, summer trends (JJA) are shown in panels b and d. Colors indicate streamflow trends.**



S4 Sub-seasonal trends in temperature, precipitation and streamflow

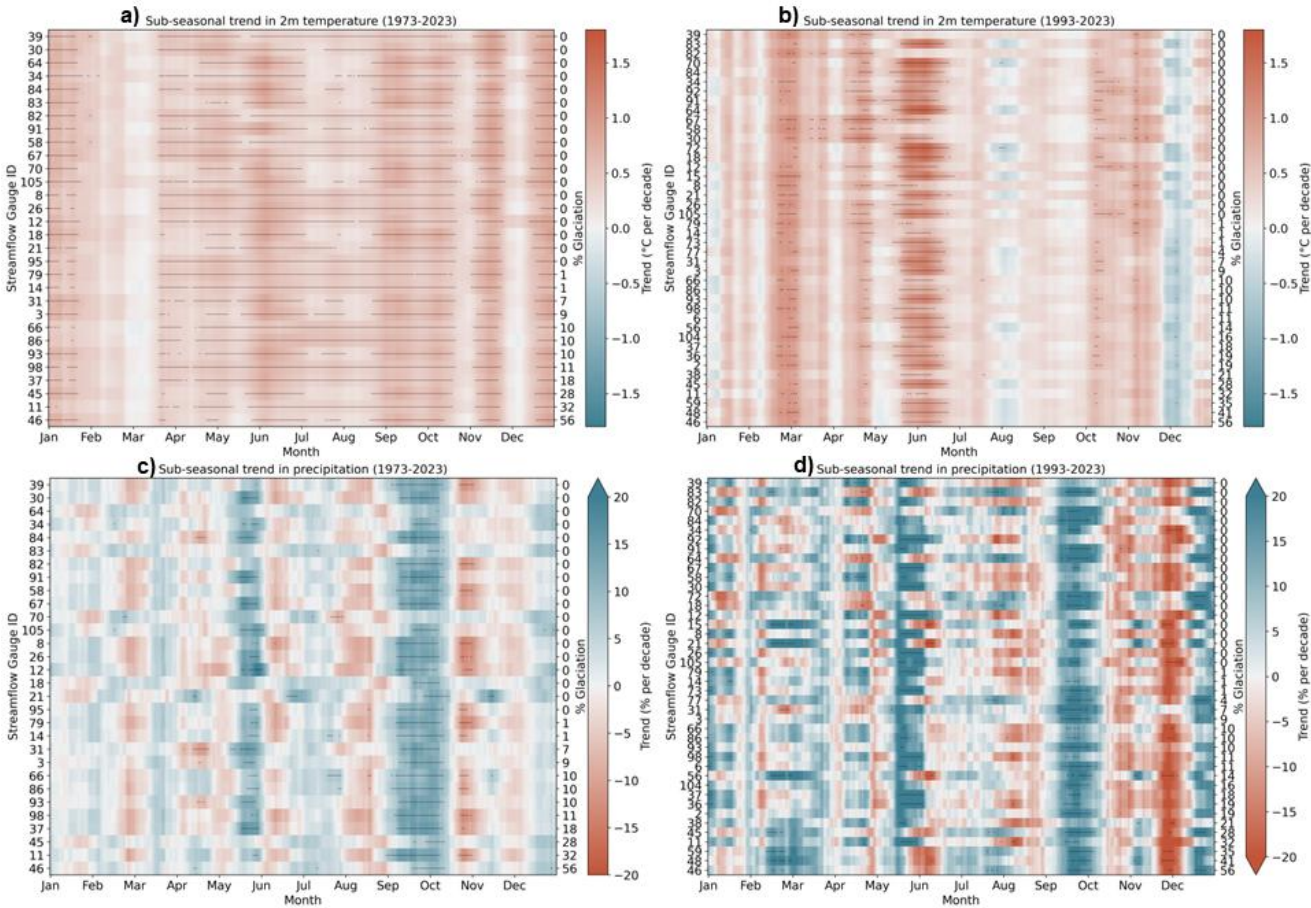


**Figure S6: Sub-seasonal trends (21DRM) in catchment-average 2m air temperature (a and b) and precipitation (c and d) from 1973-2023 and 1993-2023. An overlying dashed black line indicates that the trend is significant ( $p < 0.05$ ). Left Y-axis labels show the streamflow gauge ID number. Right Y-labels show the glaciated fraction of the catchment. The data is from the ERA5-Land reanalysis.**

Figure S6 shows the sub-seasonal trends in 2m air temperature and precipitation for periods 1 and 2. For air temperature, results for period 1 (Figure S6a) show a predominant significant positive trend in temperature for most of the year. A period in February and March exhibits the smallest (and not statistically significant) trends, along with two shorter periods in October/November and December. Trends in July and August are also small in many catchments. In contrast, results for period 2 show greater variability, including periods with negative trends (Figure S6b). Even though fewer days exhibit statistically significant trends than in period 1, the magnitude of the positive trends is notably larger. Significant increases in temperature are observed in February/March, late April and from late May to late June, while minor decreases are noted in August, December and January.





125 although positive summer trends are observed in catchments with higher glaciated fractions. Figure S7b, representing the  
period 1993-2023, exhibits a more pronounced pattern of frequent switches between positive and negative trends, with  
significant trends being fewer and more scattered throughout the year. Strong increases are particularly evident in April,  
followed by a decrease in May, indicating a shift in the timing of snowmelt. A strong increase is also evident in September to  
November. Decreases are observed from June through September for most non-glaciated catchments, and from July through  
130 September for many glaciated catchments.

135

140

145

150

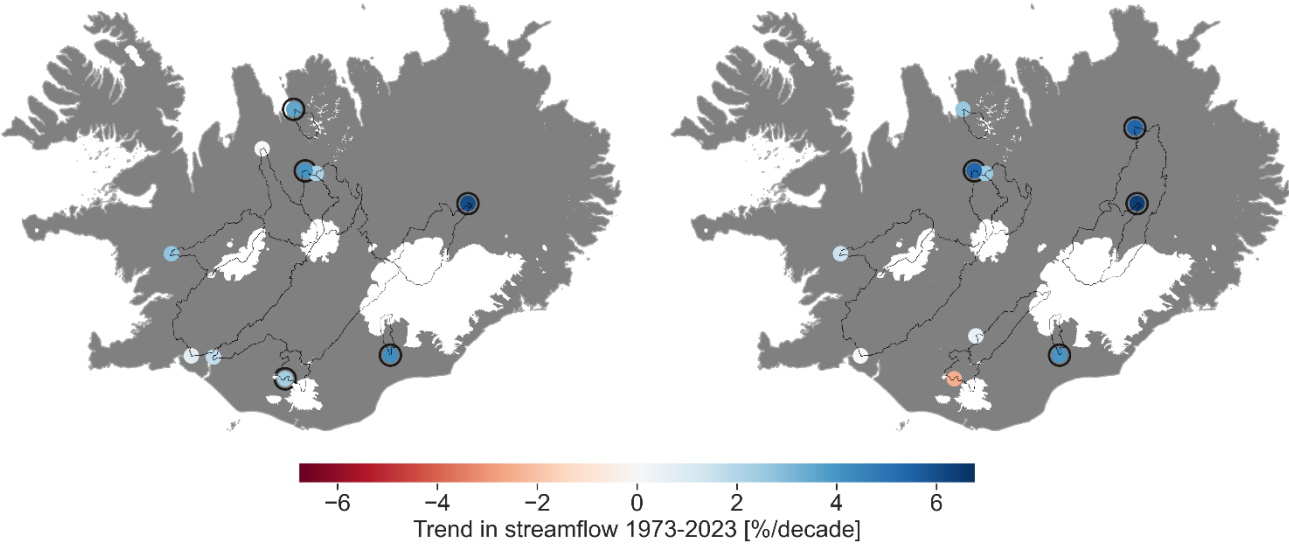
155

S5 Trends in streamflow

Figure S8 shows trends in annual and summer melt season streamflow in glacial rivers for periods 1 and 2.

a) Trend in annual average streamflow in glaciated basins  
1973-2023

b) Trend in JAS streamflow in glaciated basins  
1973-2023



c) Trend in annual average streamflow in glaciated basins  
1993-2023

d) Trend in JAS streamflow in glaciated basins  
1993-2023

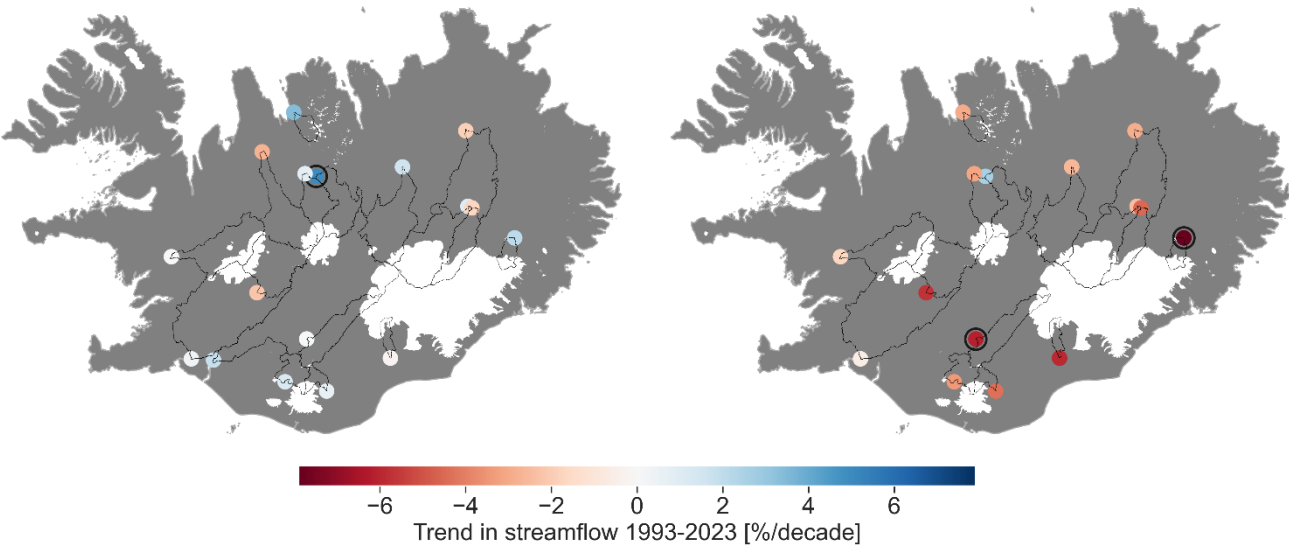
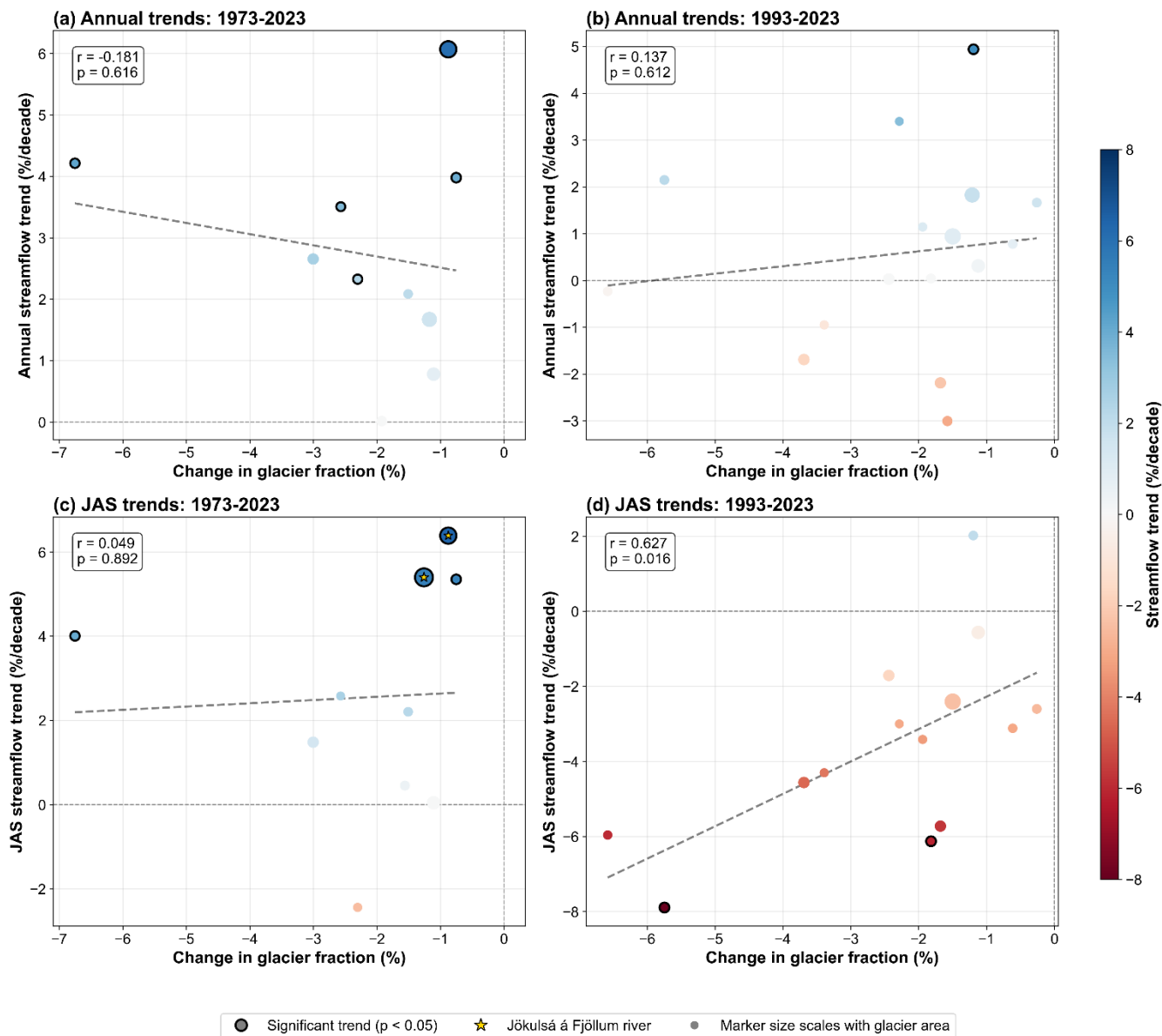
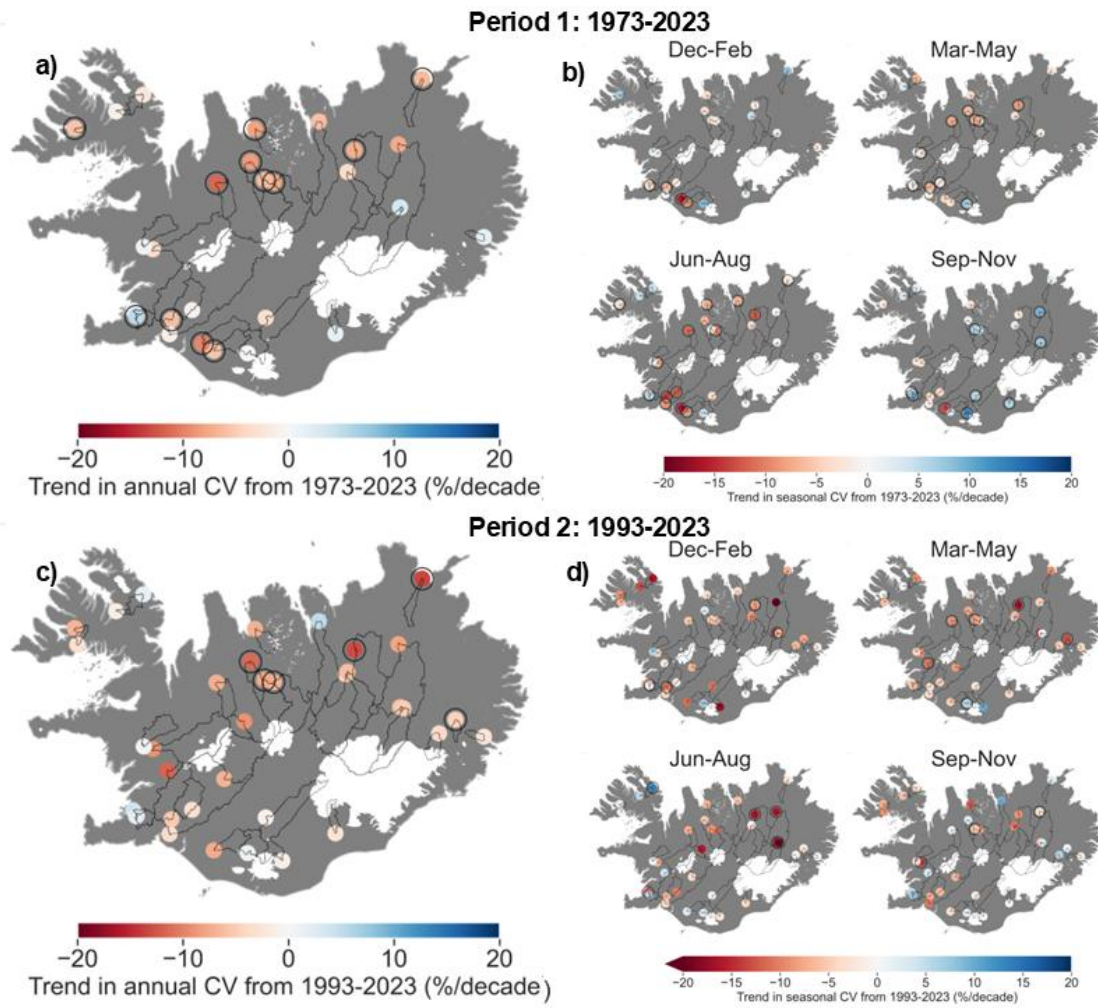


Figure S8: Trends in streamflow for gauges with more than 5% catchment glaciation. Annual trends (a, c) and summer melt season (July, August and September: b, d) in streamflow from 1973-2023 (a, b) and 1993-2023 (b, d). Black circles around gauge markers indicate statistically significant trends ( $p < 0.05$ ). Watershed outlines are shown for each gauge. Note that two gauges are located in the Jökulsá á Fjöllum river (northeast Iceland). They are only counted once in summaries in the text.



**Figure S9: Streamflow trends in glacial rivers (glacial fraction > 5%) and their relationship to changes in glaciated area.**



**Figure S10: Annual (a, c) and seasonal (b, d) trends in streamflow coefficient of variation (CV) from 1973-2023 (a, b) and 1993-2023 (b, d). Black circles around gauge markers indicate statistically significant trends ( $p < 0.05$ ). Watershed outlines are shown for each gauge.**

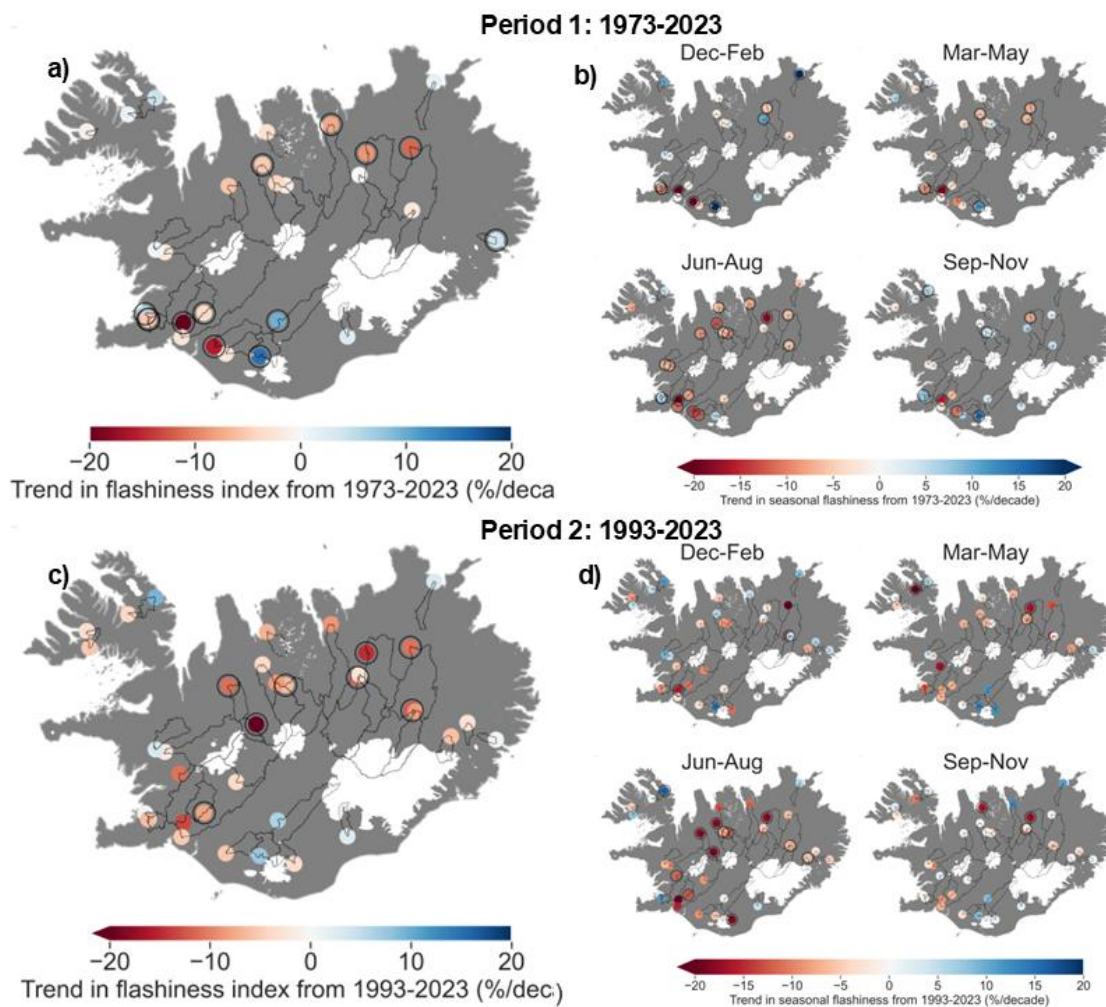
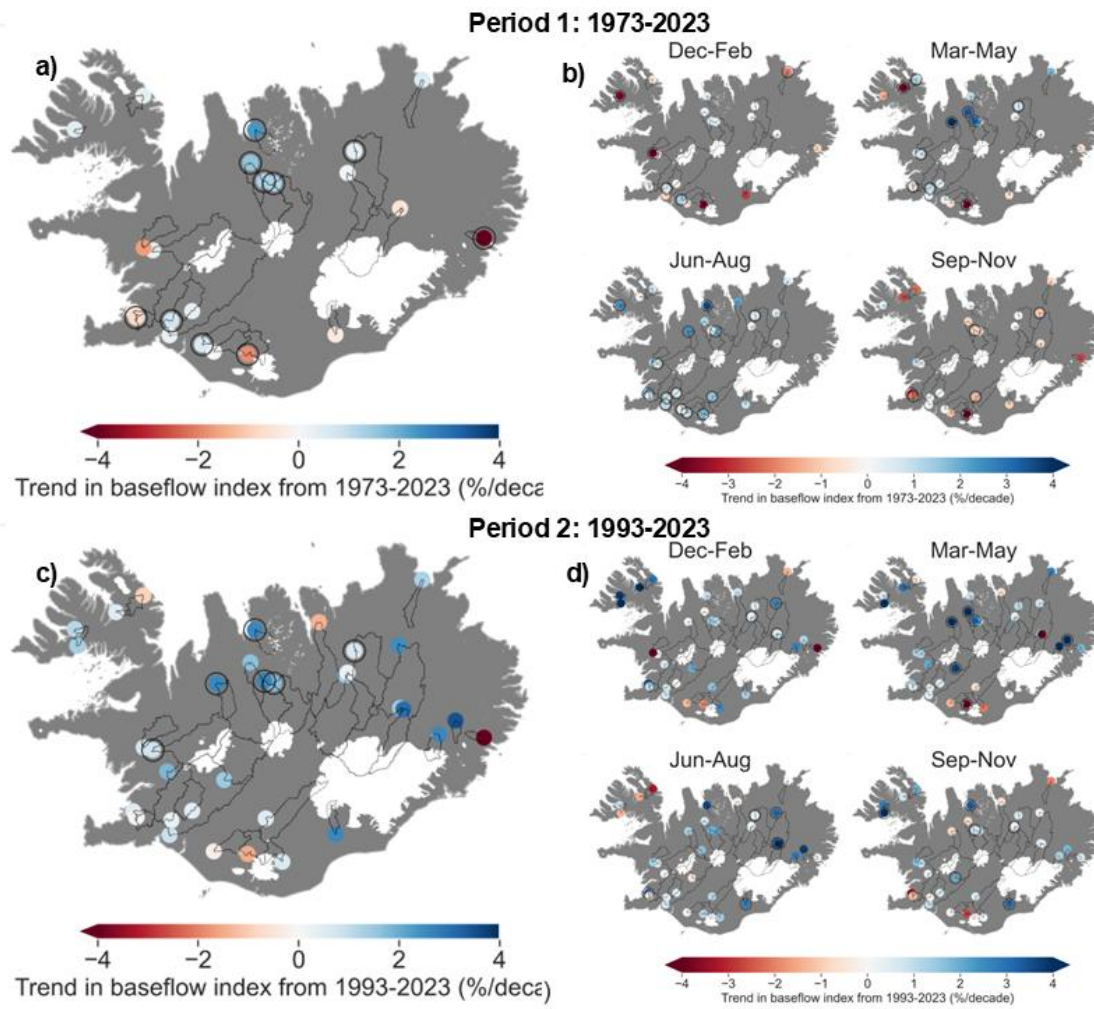


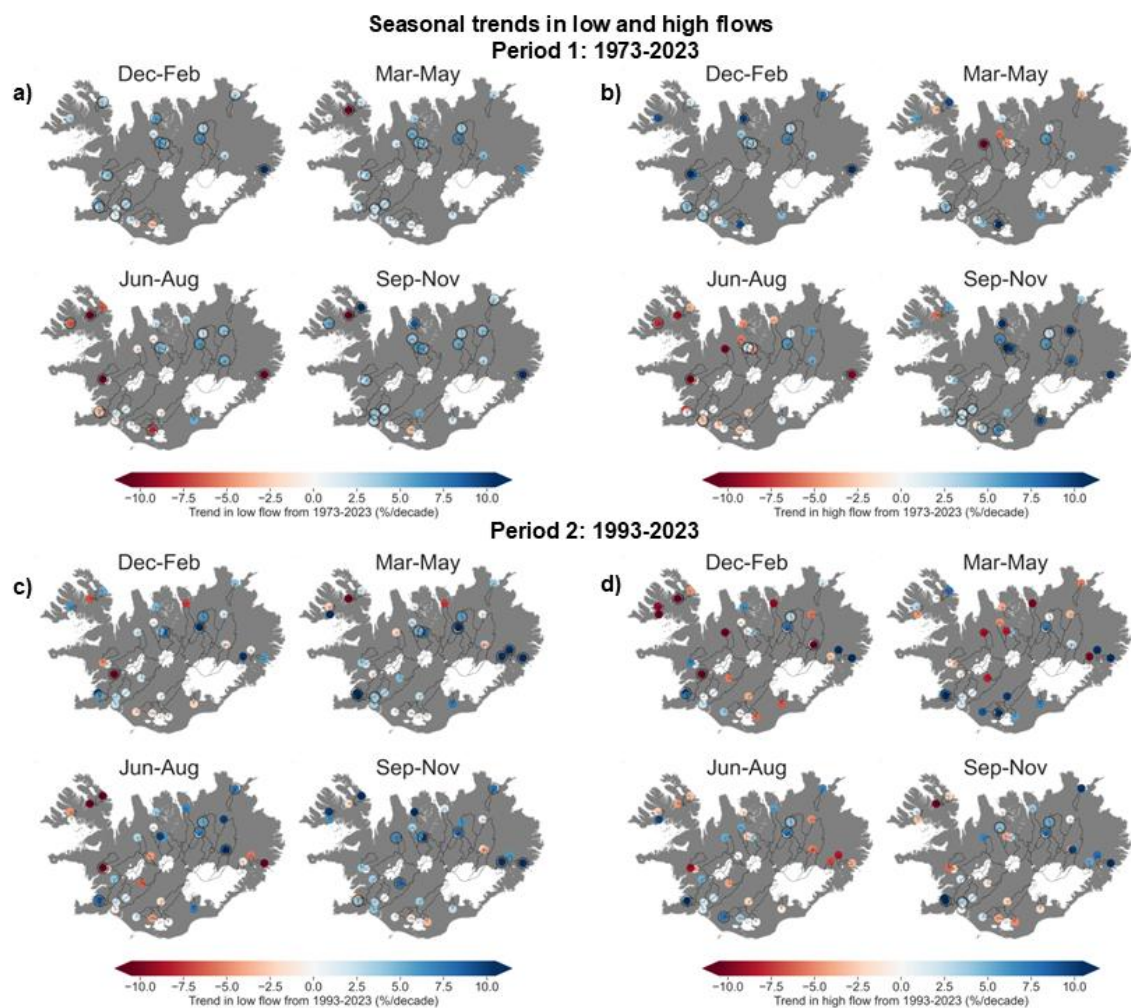
**Figure S11: Annual (a, c) and seasonal (b, d) trends in streamflow flashiness index from 1973-2023 (a, b) and 1993-2023 (b, d). Black circles around gauge markers indicate statistically significant trends ( $p < 0.05$ ). Watershed outlines are shown for each gauge.**



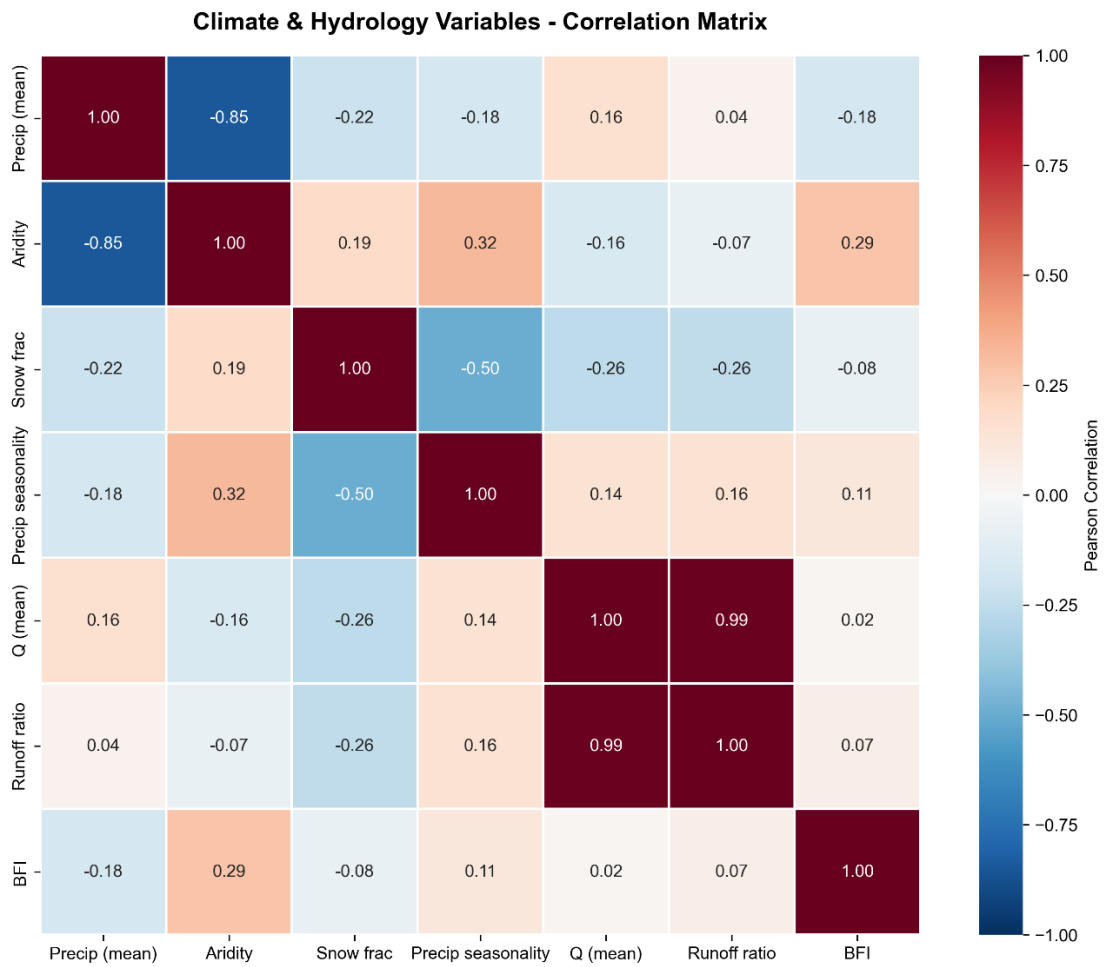


180 **Figure S12: Annual (a, c) and seasonal (b, d) trends in baseflow index from 1973-2023 (a, b) and 1993-2023 (b, d). Black circles around gauge markers indicate statistically significant trends ( $p < 0.05$ ). Watershed outlines are shown for each gauge.**





185 **Figure S13: Seasonal trends in low and high flows for periods 1 and 2. Seasonal low (a, c) and high (b, d) flows in streamflow from 1973-2023 (a, b) and 1993-2023 (b, d). Low and high flows are defined as the 10<sup>th</sup> and 90<sup>th</sup> percentiles of seasonal flow. Black circles around gauge markers indicate statistically significant trends ( $p < 0.05$ ). Watershed outlines are shown for each gauge.**



190

**Figure S14: Correlation matrix for catchment attributes - Climate and hydrology.**

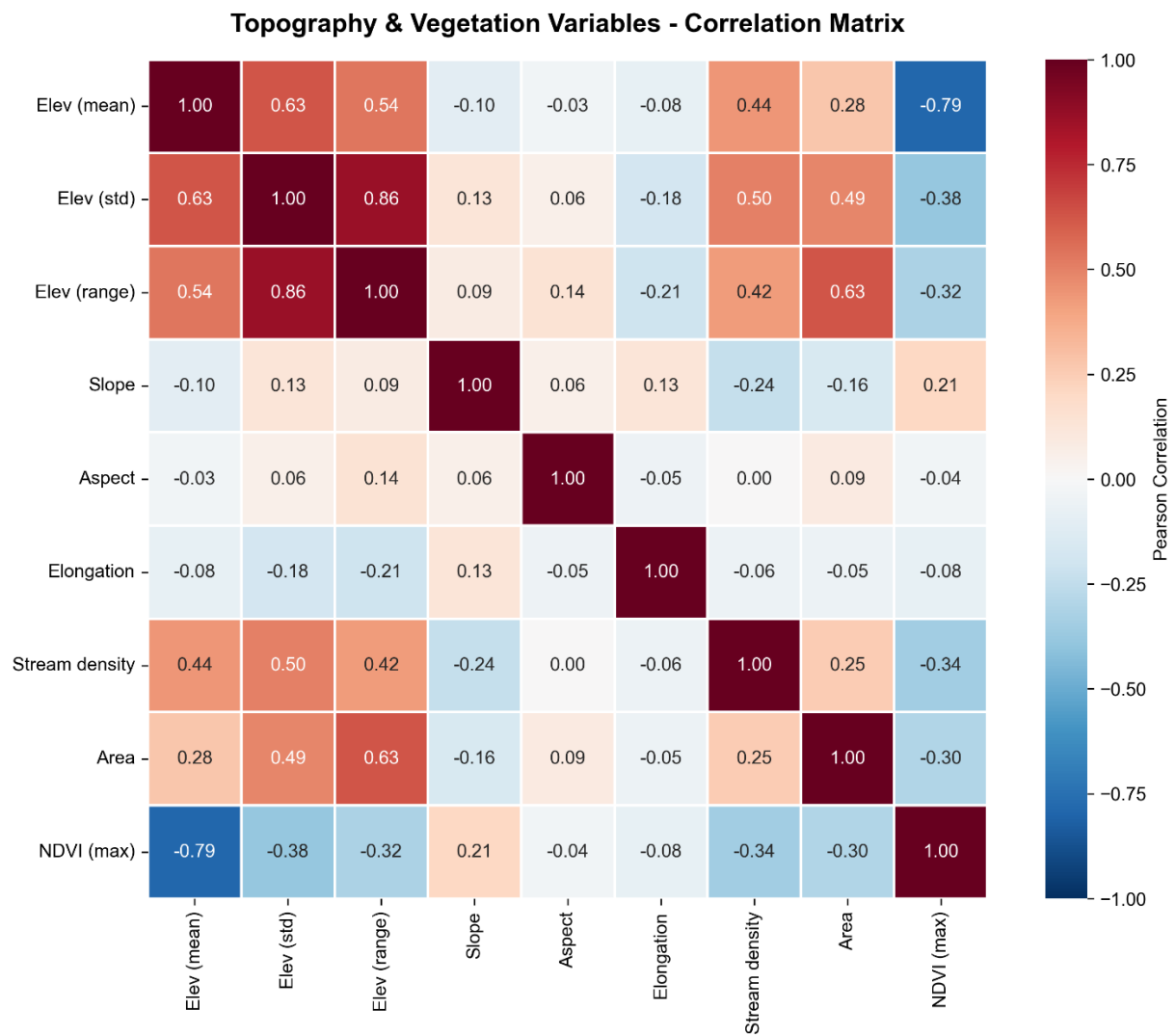


**Figure S15: Correlation matrix for catchment attributes - Topography and vegetation**

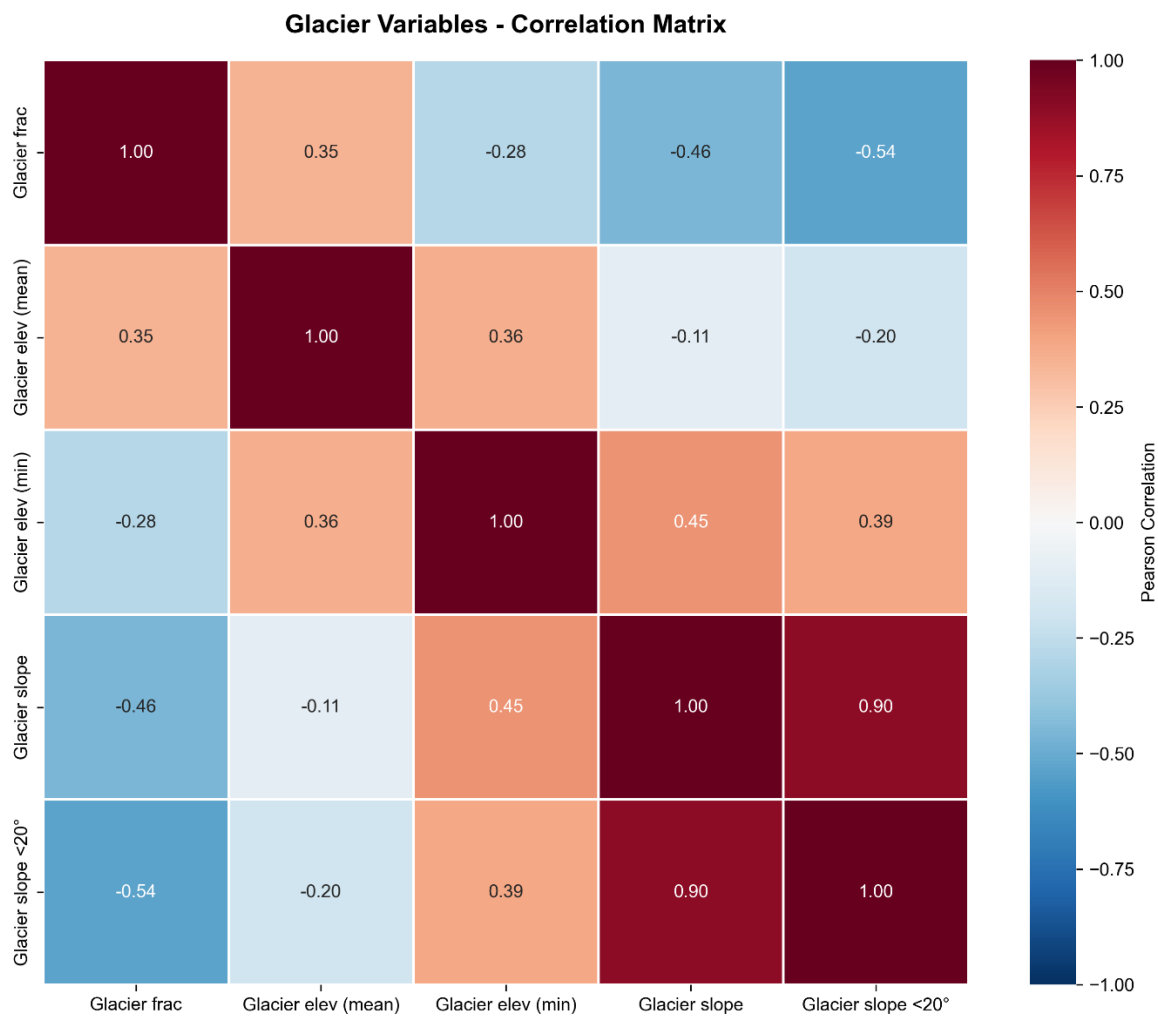


**Figure S16: Correlation matrix for catchment attributes - Glacier characteristics.**

Soil Variables - Correlation Matrix

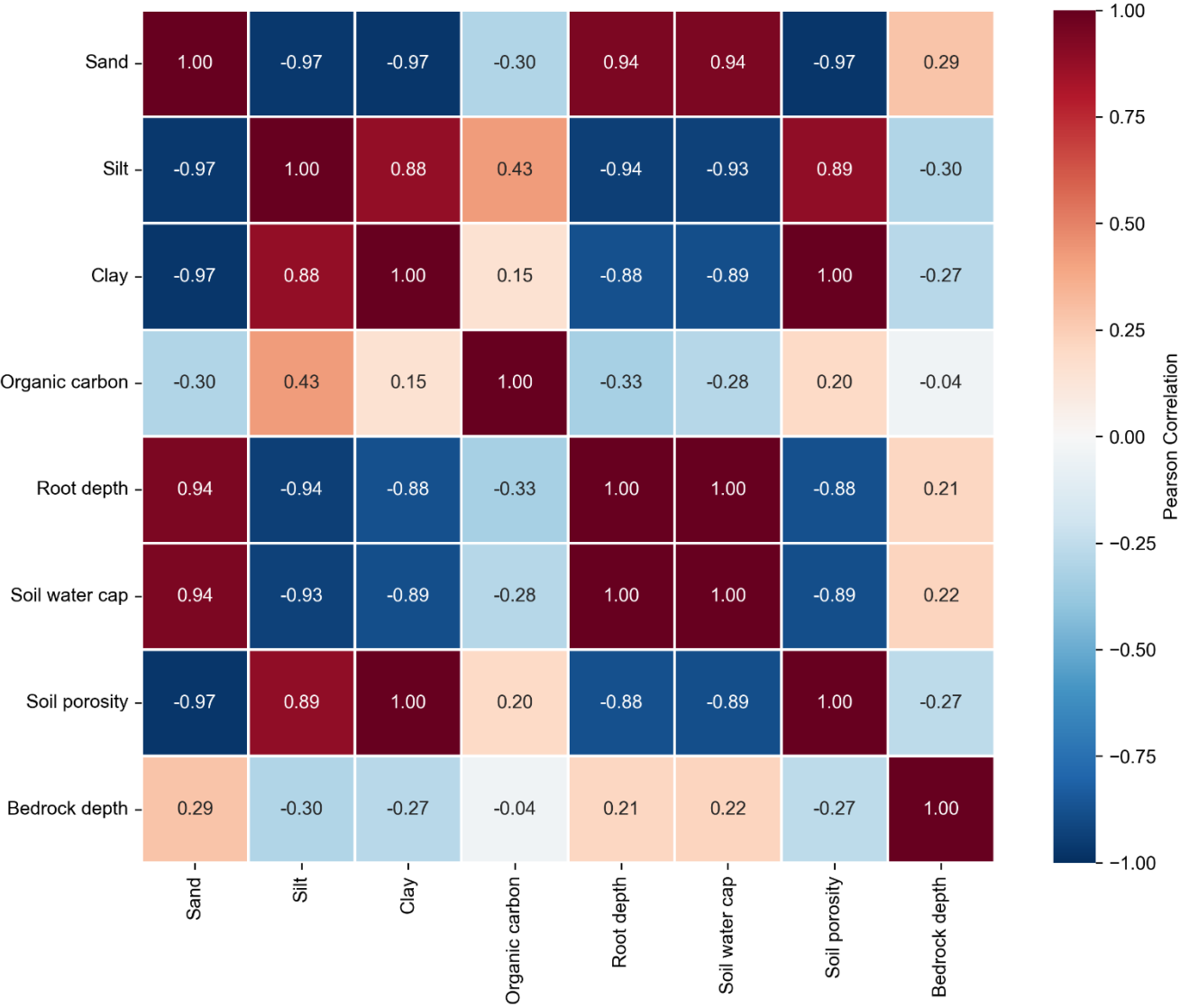
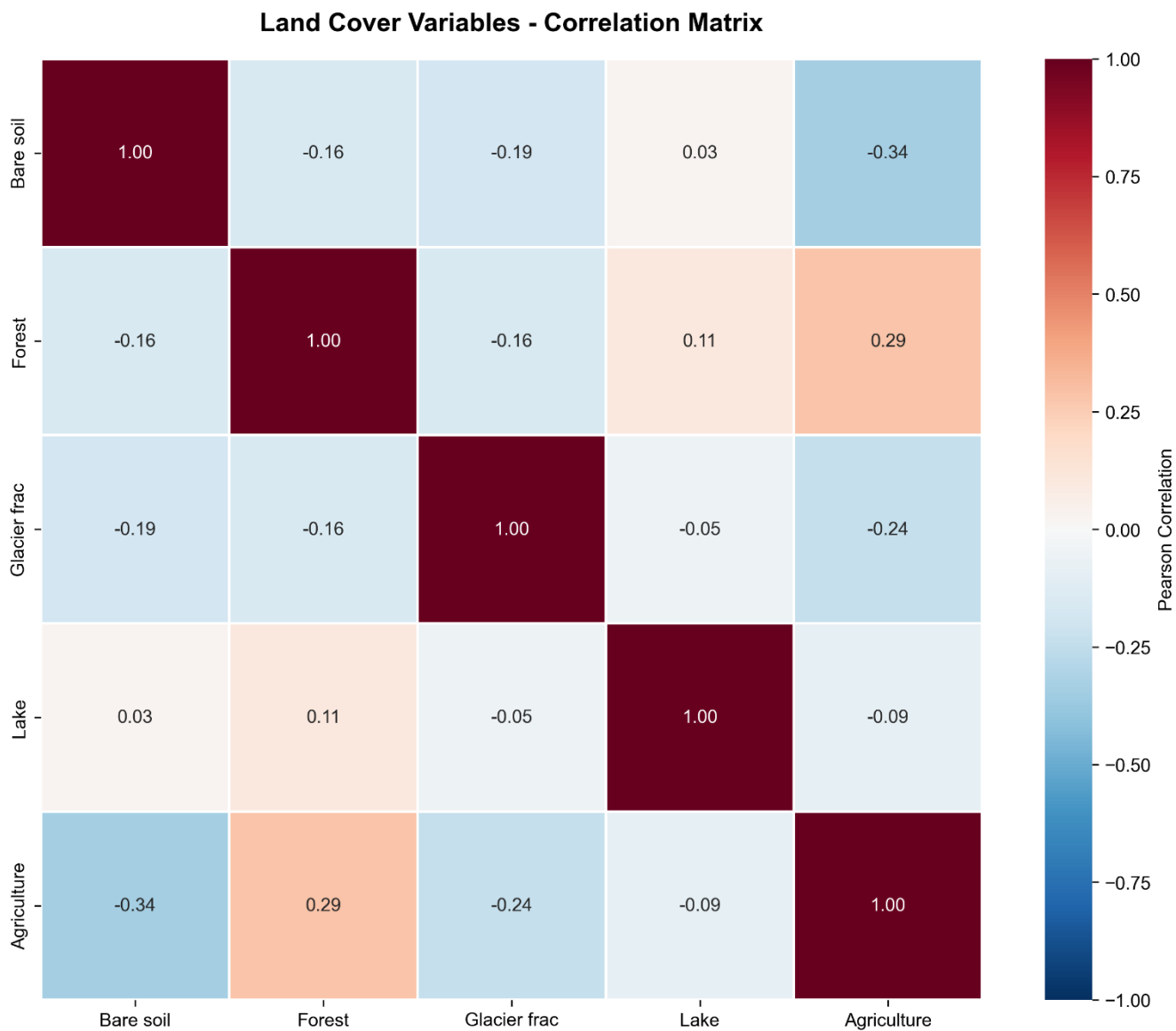
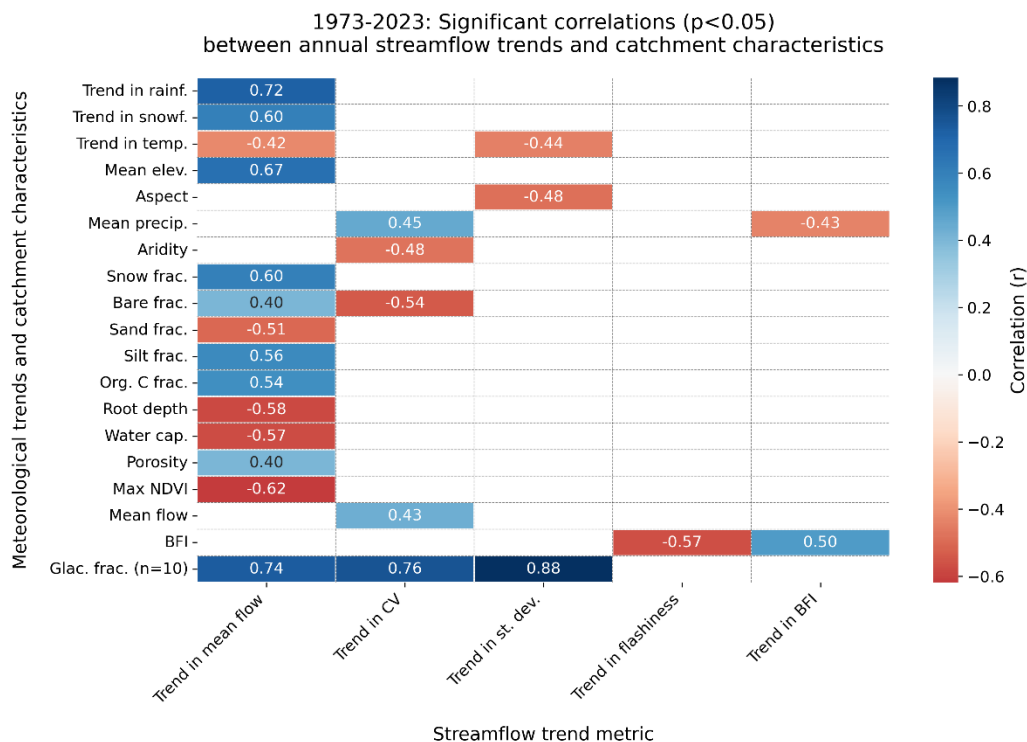


Figure S17: Correlation matrix for catchment attributes - Soil variables.



205 **Figure S18: Correlation matrix for catchment attributes - Land cover.**



210 **Figure S19: A heatmap showing significant correlations ( $p < 0.05$ ; Pearson correlation coefficient) between annual streamflow metrics and trends in meteorological variables and catchment attributes for the period 1973-2023.**

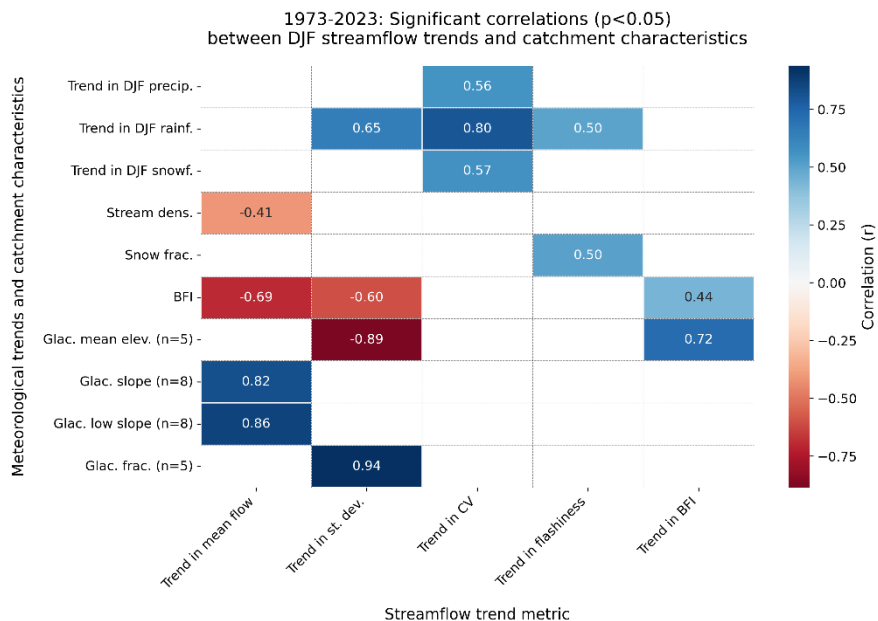
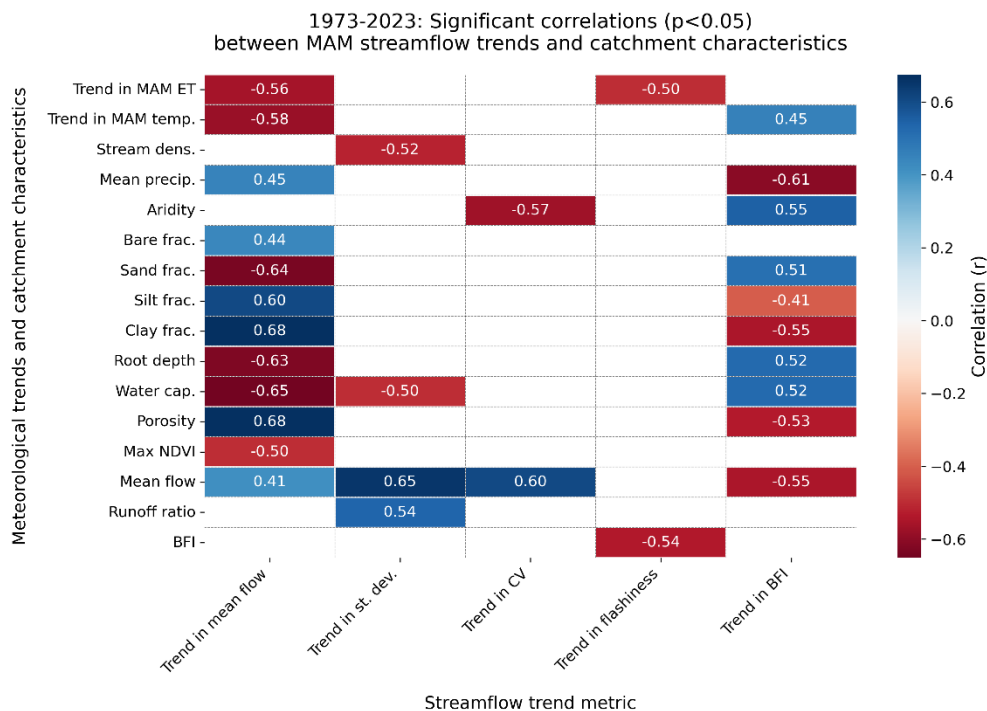
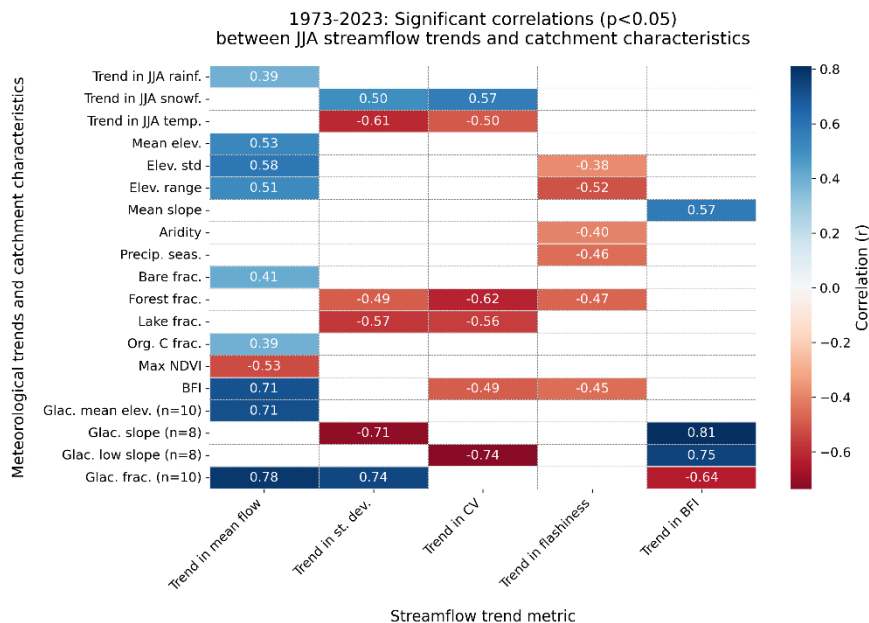


**Figure S20: A heatmap showing significant correlations ( $p < 0.05$ ; Pearson correlation coefficient) between winter (DJF) streamflow metrics and trends in meteorological variables and catchment attributes for the period 1973-2023.**





215 **Figure S21: A heatmap showing significant correlations ( $p < 0.05$ ; Pearson correlation coefficient) between spring (MAM) streamflow metrics and trends in meteorological variables and catchment attributes for the period 1973-2023.**



220 **Figure S22: A heatmap showing significant correlations ( $p < 0.05$ ; Pearson correlation coefficient) between summer (JJA) streamflow metrics and trends in meteorological variables and catchment attributes for the period 1973-2023.**

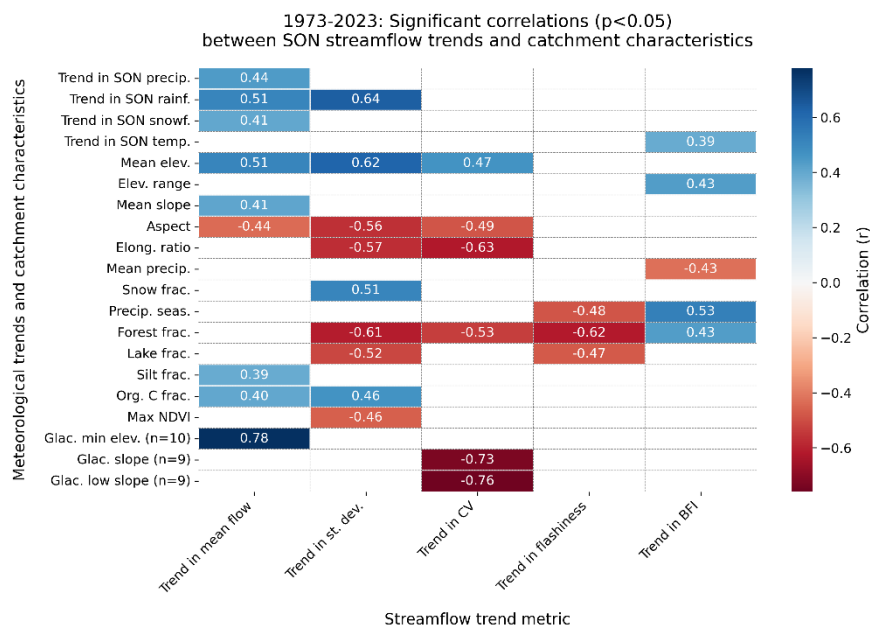
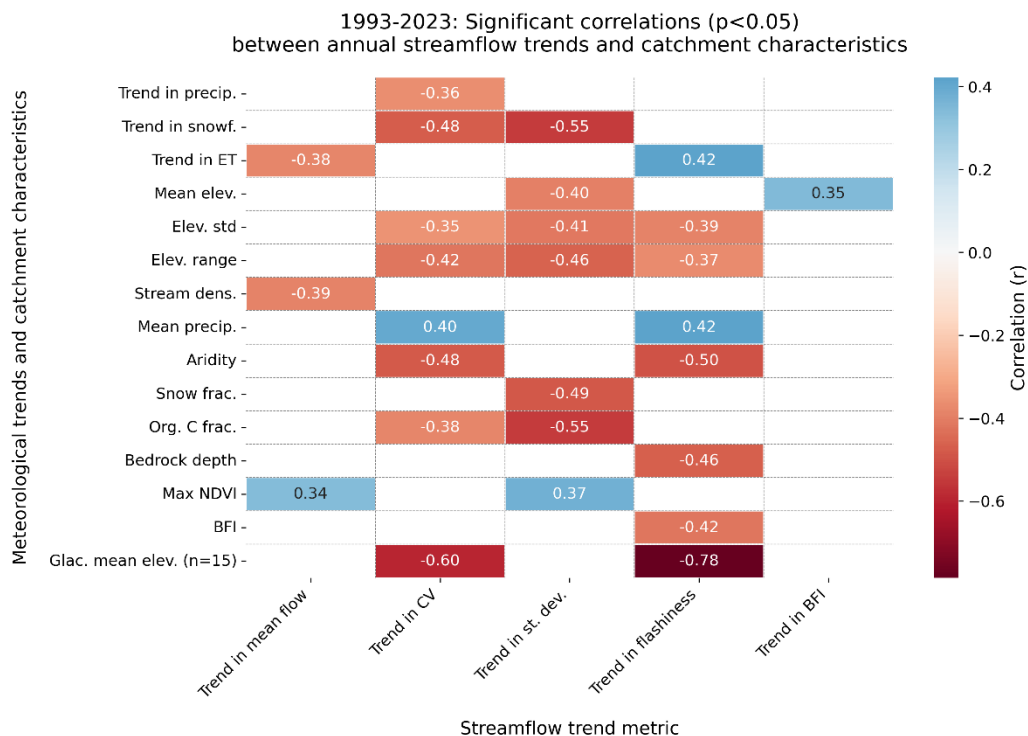


**Figure S23: A heatmap showing significant correlations ( $p < 0.05$ ; Pearson correlation coefficient) between fall (SON) streamflow metrics and trends in meteorological variables and catchment attributes for the period 1973-2023.**



230 **Figure S24: A heatmap showing significant correlations ( $p < 0.05$ ; Pearson correlation coefficient) between annual streamflow metrics and trends in meteorological variables and catchment attributes for the period 1993-2023.**

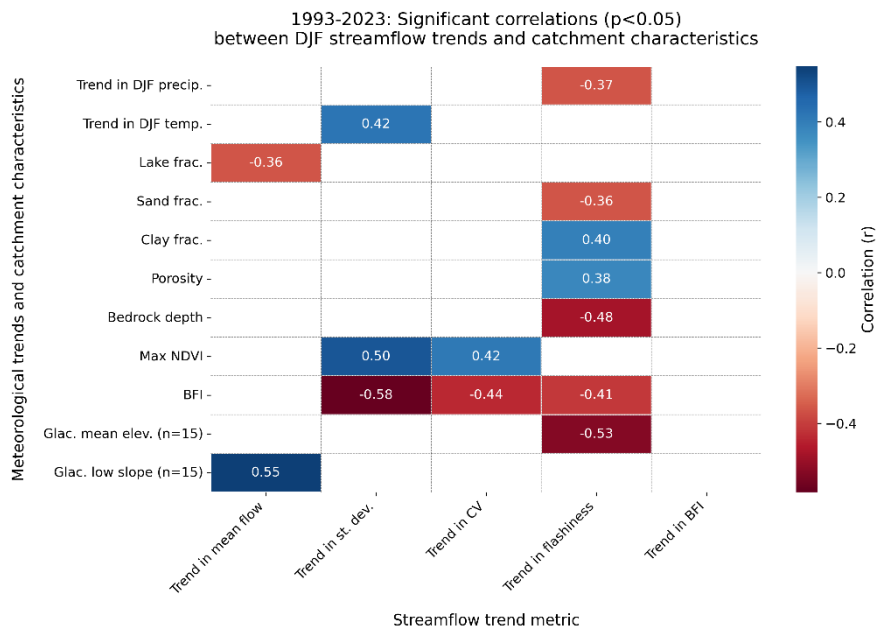
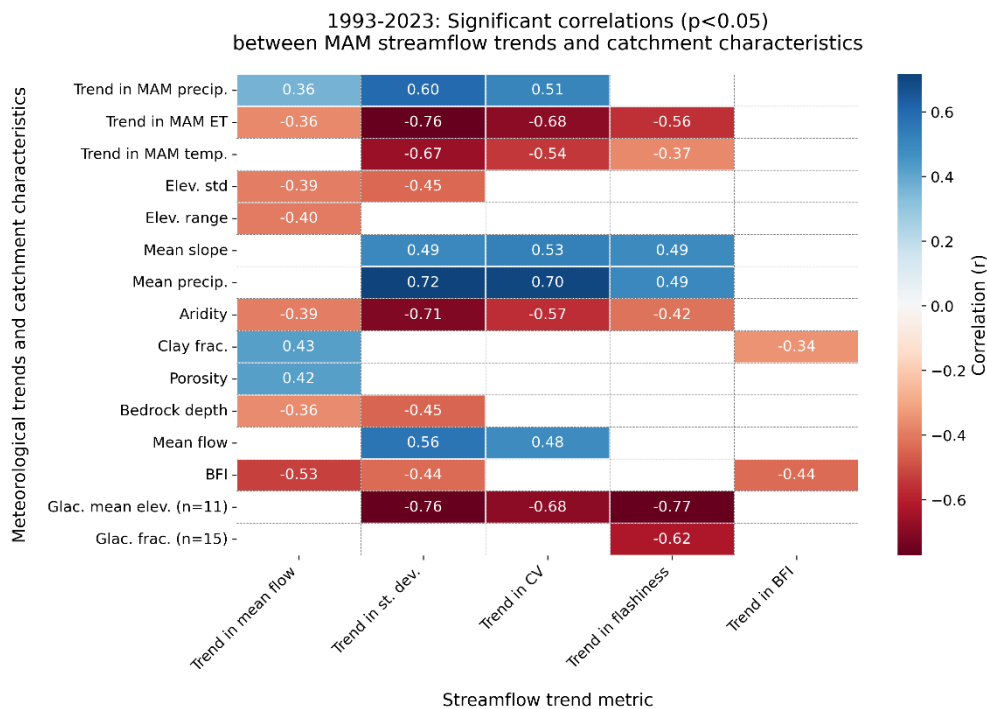
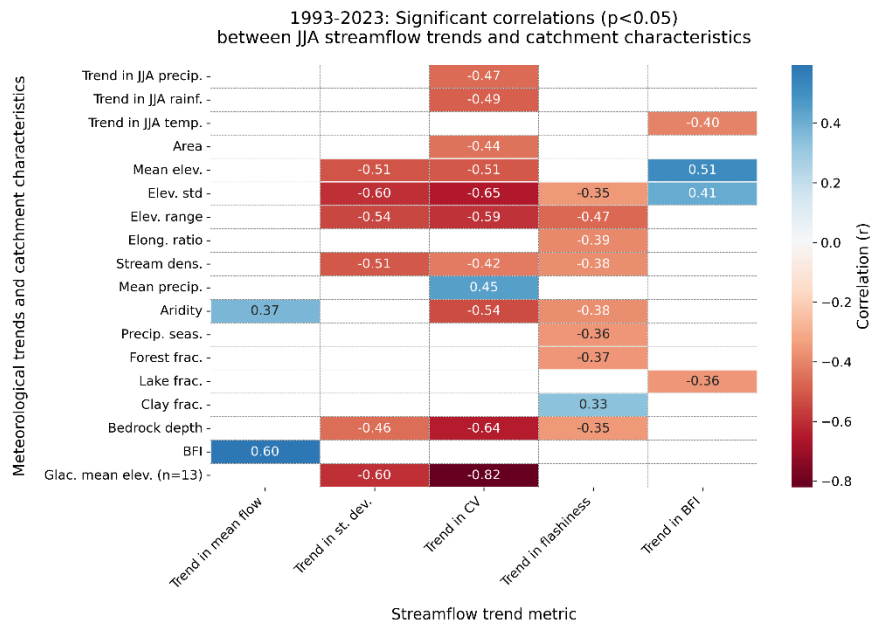


**Figure S25: A heatmap showing significant correlations ( $p < 0.05$ ; Pearson correlation coefficient) between winter (DJF) streamflow metrics and trends in meteorological variables and catchment attributes for the period 1993-2023.**



235 **Figure S26: A heatmap showing significant correlations ( $p < 0.05$ ; Pearson correlation coefficient) between spring (MAM) streamflow metrics and trends in meteorological variables and catchment attributes for the period 1993-2023.**



240 **Figure S27: A heatmap showing significant correlations ( $p < 0.05$ ; Pearson correlation coefficient) between summer (JJA) streamflow metrics and trends in meteorological variables and catchment attributes for the period 1993-2023.**

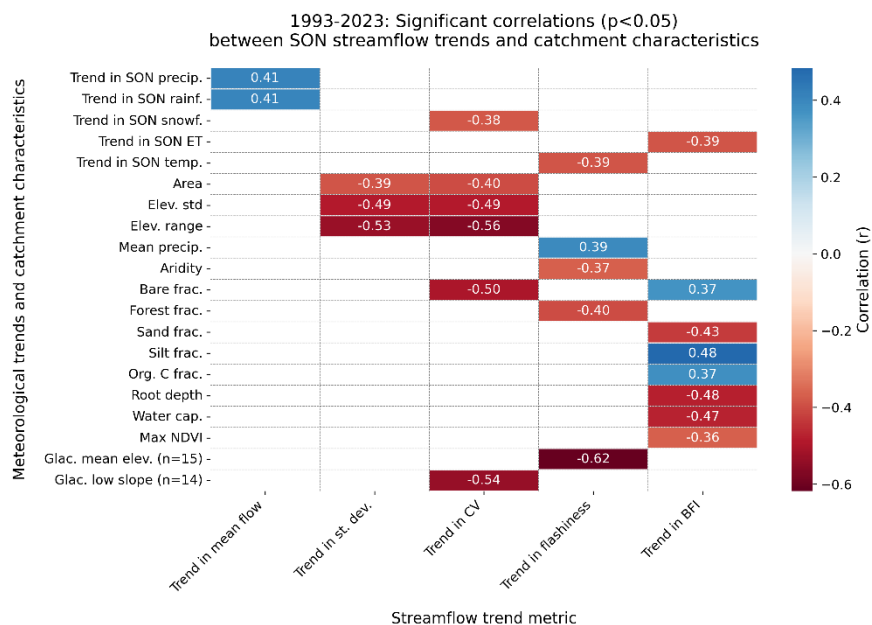


**Figure S28: A heatmap showing significant correlations ( $p < 0.05$ ; Pearson correlation coefficient) between fall (SON) streamflow metrics and trends in meteorological variables and catchment attributes for the period 1993-2023.**

S6 Overview of gauges used in the study

Streamflow gauges used in trend analysis

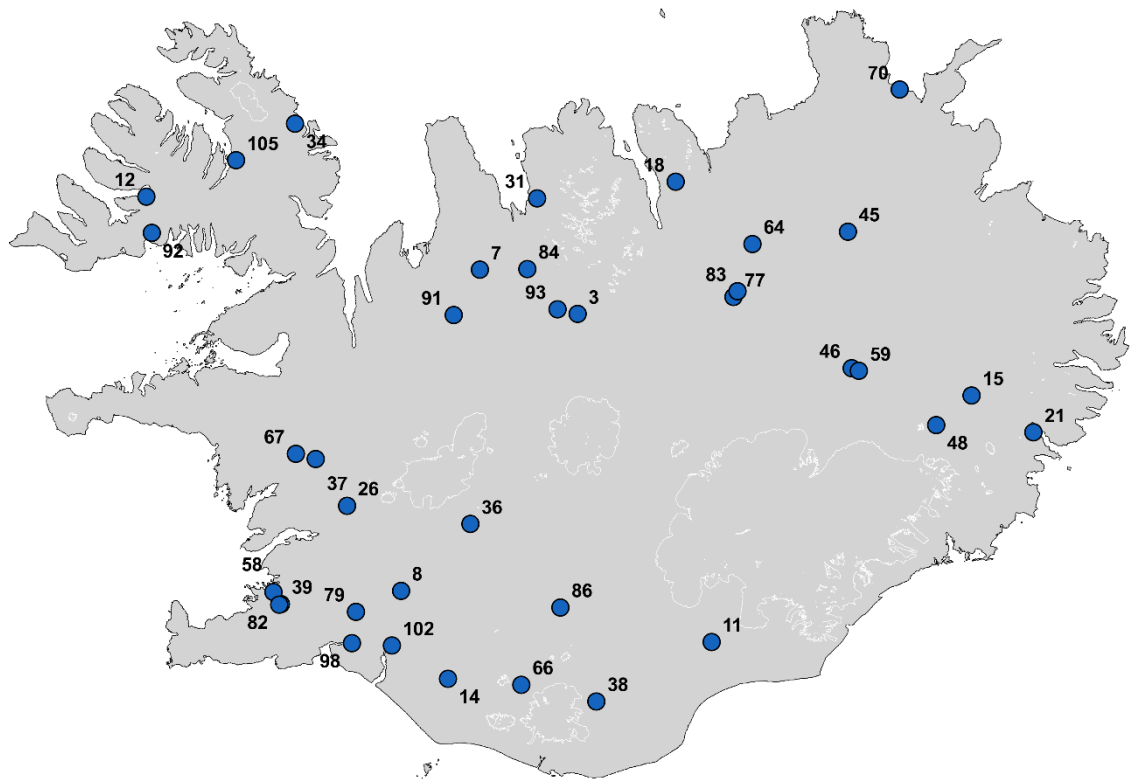


Figure S29: A map showing the location of streamflow gauges from the LamaH-Ice dataset used in the study. Gauges identified by their LamaH-Ice ID numbers.

Table S1: Overview of gauges used in this study, including river names, gauge locations, catchment areas, degree of anthropogenic impact (u: no influence, l: low influence, m: moderate influence, s: strong influence), catchment glacier percentage and percentage of years that are missing when trends in annual average flows are calculated for the two periods.

Gauge ID	River name	Station name (location)	Catchment area (km <sup>2</sup> )	Degree of impact	Catchment glacier percentage	Missing years (%) in period 1 (1973-2023)	Missing years (%) in period 2 (1993-2023)
3	Austari-Jökulsá	ofan Skatastaða	1134.9	u	8.8	2	3.2
7	Blanda	Langamýri	1673.3	s	10.4	3.9	3.2
8	Brúará	Dynjandi	642.1	l	0	2	3.2

11	Djúpá	neðan Djúpárdals	226.8	u	33.1	2	3.2
12	Dynjandisá	Sjóarfoss	42.6	l	0	7.8	6.5
14	Eystri-Rangá	Tungufoss	401.3	l	1.2	2	3.2
15	Fellsá	Sturluflöt II	125.5	u	0		16.1
18	Fnjóská	ofan Árbugsár	1129.6	u	0		12.9
21	Fossá	Eyjólsstaðir	113.5	u	0.2	7.8	12.9
26	Grímsá	Reyðarvatnsós	108.3	l	0		16.1
31	Hjaltadalsá	brú, Viðvíkursveit	299.4	u	7	9.8	16.1
34	Hvalá	Óp	192.8	u	0	7.8	3.2
36	Hvítá	Fremstaver	1665.1	l	19.4		9.7
37	Hvítá	Kljáfoss	1720	u	18.6	2	3.2
38	Hólmsá	Hólmsárfoss	237	u	21.2		3.2
39	Hólmsá	Gunnarshólmi	215.5	u	0	2	3.2
45	Jökulsá á Fjöllum	Grímsstaðir	5150.8	u	28.9		16.1
46	Jökulsá á Fjöllum	Upptypingar II	2006.7	u	56.9	19.6	6.5
48	Jökulsá í Fljótssdal	Eyjabakkafoss	302.4	u	41.5		16.1
58	Korpa	Keldnaholt	39.6	l	0	3.9	6.5
59	Kreppa	Lónshnjúkur	941.8	u	35.9		16.1
64	Laxá	Helluvað	1509.7	l	0	2	3.2
66	Markarfljót	Emstrur	516.2	u	10	19.6	3.2
67	Norðurá	Stekkur	507.4	u	0	13.7	3.2
70	Sandá	Flögubrá II	265	u	0	5.9	3.2
73	Seyðisá	Kjölur	301.7	u	1.7		
77	Skjálfandafljót	Aldeyjarfoss	1947.9	u	6.1		3.2
79	Sog	Ásgarður	997.2	m	1	2	3.2
82	Suðurá	Hófleðurshóll	3.8	u	0	2	3.2
83	Svartá	ofan Ullarfossbrúar	738.8	l	0	13.7	3.2
84	Svartá	Svartá	390.6	u	0	2	3.2
86	Tungnaá	Mariufoss	1141.1	u	10.2		3.2
91	Vatnsdalsá	Forsæludalur	449.7	u	0		12.9
92	Vatnsdalsá	Eiði	101.9	l	0		19.4
93	Vestari-Jökulsá	Goðdalabrá	842.3	u	10.5	2	3.2
98	Ölfusá	Selfoss	5724.2	l	10.8	2	3.2



102	Þjórsá	Þjórsártún	7437.2	s	12.5	2	3.2
105	Þverá	Nauteyri	44.7	u	0		19.4

**Table S2:** Streamflow (Q, m3/s), temperature (T, °C) and precipitation (P, mm/year) averages for periods 1 and 2. Streamflow is measured and temperature and precipitation are derived from the ERA5-Land reanalysis. Note that precipitation is underestimated in ERA5-Land.

Gauge ID	Q1	Q2	T1	T2	P1	P2
3	39.8	40.2	-2.3	-1.8	1045.5	1054.9
7	44.6	44.7	-1.5	-1	1077.2	1084.1
8	66.2	67.5	1.8	2.3	1847.5	1850.8
11	27.4	29.2	-1.4	-1.1	2175.2	2200.9
12	3.1	3.1	-0.2	0.3	1430.3	1433.3
14	20.8	20.6	0.7	1.2	1895.5	1923.1
15		7.7	-1.3	-0.9	1510.2	1542.7
18		38.3	-1.7	-1.3	1098.7	1120.8
21	8.4	8.7	-0.1	0.3	1666.9	1711.6
26		5.6	-0.2	0.3	1605.6	1614.3
31	11.2	11.4	-1.7	-1.2	1169.7	1186.5
34	14.8	15	0	0.4	1357.8	1381.6
36		86.6	-1.5	-1.1	1453.2	1457.4
37	82.6	85.4	-1.2	-0.8	1317.6	1326.2
38		36.9	0.2	0.6	2422.9	2480.7
39	2.1	1.9	2.1	2.6	1526.9	1544.3
45		188.6	-2.4	-2	1238.5	1252.1
46	96.3	101.6	-3.8	-3.5	1421.5	1435.7
48		26.9	-2.5	-2.1	1662	1691.3
58	1.5	1.4	2.4	2.8	1453.9	1467.6
59		45.3	-3	-2.6	1457.5	1473.5
64	38	38.7	-0.6	-0.1	1015.8	1030.1
66	43	43.7	-0.3	0.1	2173.6	2211.8
67	21.8	21.6	0.7	1.2	1163	1176.4
70	13.7	13.9	0.4	0.8	1083.7	1098
73			-1.6	-1.1	1160	1166
77		49.4	-2.2	-1.8	1133.8	1145.5
79	108.5	108.5	1	1.5	1675.5	1684.8
82	0.4	0.4	2.7	3.1	1461.4	1476
83	21.6	22.5	-1.5	-1	1127.9	1144.3
84	10.2	10.2	-0.5	0	974.6	982.6

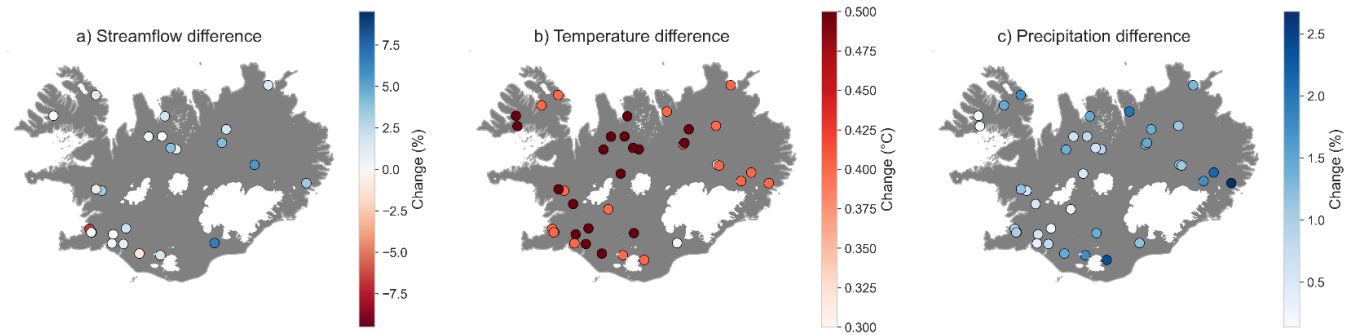
86		87.8	-0.8	-0.3	1695.2	1719.2
91		9.1	-0.5	0	987.1	1000.9
92		7.1	0.1	0.6	1455.5	1457.5
93	22.7	23.6	-1.9	-1.4	1024.1	1030.4
98	377.4	378.1	0.3	0.7	1642.5	1648.2
102	350.2	353.4	-1	-0.5	1446.2	1457.7
105		2.4	-0.1	0.3	1315.5	1334.5
Mean	59.4	60.2	-0.6	-0.2	1430.8	1447.3

260

From Table S2, the difference in mean streamflow between Period 1 (59.4 m³/s) and Period 2 (60.2 m³/s) corresponds to a 1.3 % change when comparing the overall averages. When calculated as the average of the percent changes at individual stations, the mean change is slightly lower at 0.89 %. Precipitation shows a similar pattern: the difference between the two period means (1430.8 vs. 1447.3 mm yr<sup>-1</sup>) corresponds to a 1.2 % change, while the average of the percent changes at individual stations is 1.12 %. Temperature increased by an average of 0.4 °C between the two periods. Figure S23 illustrates the spatial distribution of these changes, with the largest increases in precipitation and streamflow occurring in eastern catchments and weakening towards the west, while the smallest temperature differences are observed in eastern Iceland.

265

Regional differences in averages between periods (Period 2 - Period 1)



270

**Figure S30: Streamflow, temperature and precipitation regional average changes between periods 1 and 2.**

**References**

Fleig, A. K., Andreassen, L. M., Barfod, E., Haga, J., Haugen, L. E., Melvold, K., Hisdal, H., and Saloranta, T.: Norwegian Hydrological Reference Dataset for Climate Change Studies, Norwegian Water Resources and Energy Directorate, Oslo, Technical report, ISBN: 978-82-410-0869-6, 2013.

275

Hussain, M. M., Mahmud, I., and Bari, S. H.: pyHomogeneity: A Python Package for Homogeneity Test of Time Series Data, J Open Res Softw, 11, <https://doi.org/10.5334/JORS.427>, 2023.

280 Pettitt, A. N.: A Non-Parametric Approach to the Change-Point Problem, J R Stat Soc Ser C Appl Stat, 28, 126–135, <https://doi.org/10.2307/2346729>, 1979.

Rögnvaldsson, Ó., Chang, H., Stanislawska, K., and Okrzesa, M.: Comparison of observed and simulated weather - Description of three dynamical downscaling experiments and comparison with observations, Technical report, available at <http://ftp.belgingur.is/publications/ObsSim-comparison-TechReport2025.pdf>, 2025.